Some thoughts on Darcy-type flow simulation for modelling underground CO_2 storage, based on the Sleipner CO_2 storage operation

G.A. Williams[a,*], R.A. Chadwick[b], H. Vosper[b]

[a] British Geological Survey, Murchison House, West Mains Road, Edinburgh, EH9 3LA, United Kingdom
[b] British Geological Survey, Environmental Science Centre, Nicker Hill, Keyworth, Nottingham, NG12 5GG, United Kingdom

ARTICLE INFO

ABSTRACT

We take three flow simulators, all based on Darcy's Law but with different numerical solver implementations, to assess some of the issues surrounding their use to model underground CO_2 storage. We focus on the Sleipner CO_2 injection project, which, with its seismic monitoring datasets, provides unique insights into CO_2 plume development during a large-scale injection operation. The case studies firstly compare simulator performance in terms of outputs and run-times on carefully matched model scenarios; then we compare numerical with analytical Darcy solutions to explore the potential for modelling simplification; finally we look at the effects of including conservation of energy in the simulations. The initial case-study used simplified axisymmetric model geometry to simulate the upward flux of CO_2 through a heterogeneous reservoir, incorporating multiphase flow with coupled CO_2 dissolution into formation brine. All three codes produced near-identical results with respect to CO_2 migration velocity and total upward CO_2 flux at the reservoir top. The second case-study involved 3D modelling of the growth of the topmost layer of CO_2 trapped and migrating beneath topseal topography. Again the three codes showed excellent agreement. In the third case-study the simulators were tested against a simplified analytical solution for gravity currents to model the spreading of a single CO_2 layer beneath a flat caprock. Neglecting capillary effects, the numerical models showed similar layer migration and geometry to the analytical model, but it was necessary to minimise the effects of numerical dispersion by adopting very fine cell thicknesses. The final case-study was designed to test the non-isothermal effects of injecting CO_2 into a reservoir at non-ambient temperature. Only two of the simulators solve for conservation of energy, but both showed a near identical thermal anomaly, dominated by Joule-Thomson effects. These can be significant, particularly where reservoir conditions are close to the critical point for CO_2 where property variations can significantly affect plume mobility and also seismic response. In conclusion, the three simulators show robust consistency, any differences far less than would result from geological parameter uncertainty and limitations of model resolution. In this respect the three implementations are significantly different in terms of computing resource requirement and it is clear that approaches with simplified physics will pay rich dividends in allowing more detailed reservoir heterogeneity to be included. Contrary to this, including conservation of energy is heavier on computing time but is likely to be required for storage scenarios where the injectant stream is significantly different in temperature to the reservoir and most critically for shallower storage reservoirs where CO_2 is close to its critical point.

1. Introduction

Numerical simulations are a vital tool for understanding the short, medium and long-term fate of CO_2 injected in the subsurface. Indeed, one of the key regulatory requirements outlined in the European Directive on CO_2 storage (EU, 2009) is to demonstrate "…. conformity of the actual behaviour of the injected CO_2 with the modelled behaviour". It is important therefore to determine the validity and applicability of numerical simulators for reproducing the key coupled processes related to flow of CO_2 in the reservoir.

Here we look at three commonly used numerical simulators to assess their efficacy for modelling underground CO_2 storage. The assessment is in three parts. First we test the comparative performance of the simulators on two identical model scenarios – one with axisymmetric geometry, one with full 3D geometry. Second we compare the numerical results with analytical solutions for a spreading CO_2 layer. Finally we assess the degree to which it is necessary to include thermal effects in CO_2 flow simulation.

Various authors (e.g. Pruess, 2005; Class et al., 2009) have run code comparisons on CO_2 injection problems; some have focussed on hypothetical test cases and others such as Singh et al. (2010) have utilised calibration data from a real injection project. In all these cases a satisfactory match between the codes was obtained but with some differences that can largely be ascribed to variation in modelling implementation between the operators at the various institutes carrying out the code comparison.

Our comparison differs somewhat from previous studies in that all three simulators were tested in-house (at BGS), with model meshes carefully designed to be as identical and/or equivalent as practicable. In this way, modelling differences due to 'operator-effect' were largely eliminated.

For this study we deployed three simulators: TOUGH2 from Lawrence Berkeley National Laboratory (Pruess, 2004); ECLIPSE 100 the industry-standard black oil simulator from Schlumberger (Schlumberger 2011); PFLOTRAN an open-source parallel subsurface flow and reactive transport code (Lichtner et al., 2015). All three are based on established multi-phase implementations of Darcy's Law for fluid flow in a porous medium.

The CO_2 storage project at Sleipner (Baklid et al., 1996) has a comprehensive time-lapse seismic monitoring programme which provides unique detail on large-scale CO_2 plume development. The case-study simulations presented here are based around these monitoring results, for overall realism, and to enable us to explore some of the issues around the numerical simulation of actual physical processes. But it is important to stress that we do not attempt to obtain exact history-matches of the Sleipner monitoring data; this is a multi-faceted task outside the scope and aims of our comparative study.

1.1. The Sleipner CO_2 storage operation

CO_2 separated from natural gas produced at the Sleipner field in the North Sea (Norwegian block 15/9) is being injected into the Utsira Sand, a regional saline aquifer of late Cenozoic age (Fig. 1). The aquifer comprises mostly unconsolidated sand of high porosity ($> 30\%$) and high permeability (> 1 Darcy) and is generally in excess of 200 m thick in the Sleipner area. A number of thin intra-reservoir mudstones, typically 1–2 m thick, are evident from geophysical logs acquired in wells around Sleipner (Fig. 1).

The CO_2 is injected via a deviated well in a dense phase at a depth of 1012 m below sea level, approximately 200 m below the top of the aquifer. Injection commenced in 1996 at a roughly constant rate, with around 15 million tons of CO_2 stored by 2016. The growth of the resulting plume has been monitored using repeat time-lapse 3D seismic data acquired in 1999, 2001, 2002, 2004, 2006, 2008 and 2010 (Fig. 2).

The CO_2 is imaged on the seismic data as a number of high amplitude sub-horizontal reflections within the reservoir (Fig. 2). Most of this reflectivity is thought to arise from thin layers of CO_2 trapped beneath the intra-reservoir mudstones which are partially but not wholly sealing (Arts et al., 2008; Chadwick et al., 2004, 2005, 2010; Chadwick and Noy, 2015; Chadwick et al., 2016). The seismic data suggest that CO_2 has migrated vertically upwards through the reservoir via a chimney in the mudstones (Fig. 2) located a little to the south of the injection point. Nine interpreted reflective layers had formed by 1999 (when CO_2 first reached the top of the reservoir), and each individual reflective layer has remained mappable on all of the subsequent surveys.

1.2. Simulators used in the code comparison

ECLIPSE 100 is a fully implicit, 3D, 3-phase, isothermal black oil simulator. Fluid Pressure-Volume-Temperature (PVT) properties are interpolated from look-up tables as a function of pressure. The simulations in this code comparison were run using block-centred geometry (Schlumberger, 2011), with inter-block transmissibility calculated using an arithmetic average of the cell interface area coupled with the
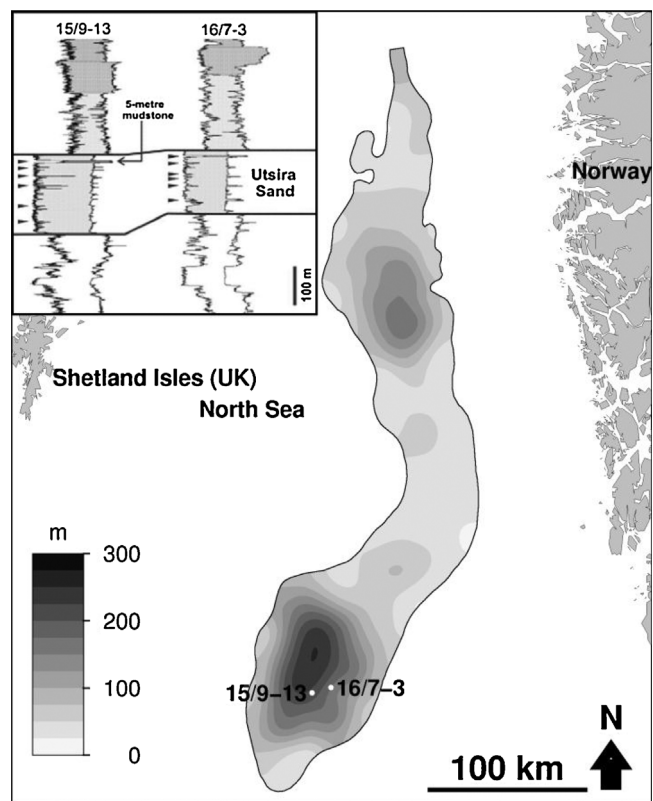

Fig. 1. Isopach map of the Utsira Sand and (inset) representative geophysical well logs showing reservoir heterogeneity (γ-ray logs on the left tracks and resistivity logs on the right tracks). The reservoir sand has characteristically low γ-ray and resistivity readings so peaks within the sand denote thin mudstones.

harmonic average of the permeability. The density and compressibility of CO_2 as a function of temperature were calculated using the Span and Wagner (1996) equation-of-state and converted to the relevant black oil representation using the scheme published by Hassanzadeh et al. (2008): brine is represented as an oil phase in the simulator, allowing for CO_2 dissolution. Activity coefficients for CO_2 and H_2O were obtained directly from the equation-of-state using the methodology described by Spycher and Pruess (2005), while the solubility of CO_2 in brine was calculated according to Duan et al. (2006). Brine density and viscosity were taken from the International Association for the Properties of Water and Steam tables, using Ezrokhi's method to calculate the density effect of salt and dissolved CO_2 (Zaytsev and Aseyev, 1992). The viscosity of CO_2 was calculated as a function of temperature and density using relationships published by Vesovic et al. (1990) and Fenghour et al. (1998).

TOUGH2 was designed as a general purpose, multi-phase, non-isothermal simulator (Pruess et al., 1999; Pruess, 2004). It uses integral finite differences to achieve spatial discretisation, with fully implicit time stepping. By default it implements an upstream weighting scheme to calculate inter-node transmissibility coefficients, but this was changed to a harmonic averaging scheme to match the ECLIPSE models. The code comparison used the ECO2N fluid properties module (Pruess, 2005), which uses the methodology described by Spycher and Pruess (2005) to compute activity coefficients. CO_2 density and viscosity are derived from correlations published by Altunin (1975); which provide a very close approximation to the Span and Wagner (1996) equation-of-state. These PVT correlations are used to generate tables of CO_2 and brine properties that are then interpolated during the computation to obtain specific phase parameters. The solubility of CO_2 in brine is calculated according to Duan et al. (2006).

PFLOTRAN is an open-source, parallel subsurface flow and reactive transport code, built on top of the PETSc family of PDE numerical
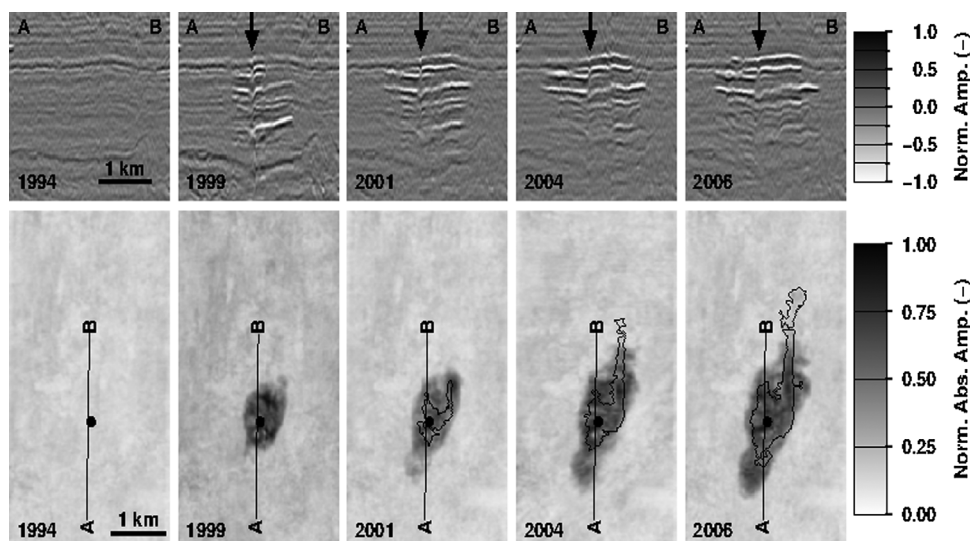
Fig. 2. Cross-section from the time-lapse 3D seismic data at Sleipner showing the baseline (1994) dataset and selected repeat surveys. The amplitudes have been normalised using the maximum survey amplitude to facilitate comparison between vintages. Note strong reflections corresponding to the CO_2 plume (top panels). Maps of the plume expressed as normalised average absolute reflection amplitude in a travel-time window containing the plume (bottom panels). Line of cross-section is marked with a black line in map view. Location of the plume feeder chimney is indicated by a black circle in map view and a black arrow on the seismic sections. Black polygons from 2001 onwards mark the extent of the topmost CO_2 layer within the overall plume footprint.

solvers (Lichtner et al., 2015). It contains a specific multiphase model of the brine − CO_2 fluid system (MPHASE), with CO_2 density calculated using the Span and Wagner (1996) equation-of-state. MPHASE calculates the viscosity of CO_2 as a function of temperature and density using relationships published by Fenghour et al. (1998). Again, the solubility of CO_2 in brine is calculated according to Duan et al. (2006). PFLO-TRAN uses the International Formulation Committee of the Sixth International Conference on Properties of Steam (Haywood, 1965) to compute the density and viscosity of water. These PVT correlations are used to generate tables of CO_2 and brine properties that are then interpolated during the computation to obtain specific phase parameters.

1.3. Reservoir and fluid properties

Reservoir temperatures were based on robust long-term measurements from the nearby Volve water production operation, quoted in Alnes et al. (2011). Reservoir pressures were assumed to be initially hydrostatic. Internal fluid property modules supplied with TOUGH2 and PFLOTRAN were used to compute the density and viscosity of CO_2 as a function of temperature and pressure (see above), with example values shown in Table 1. Brine fluid properties were calculated for a sodium chloride mass fraction of 0.032, giving a mean brine density and viscosity of approximately $1020 \, \mathrm{kg \, m^{-3}}$ and 8×10^{-4} Pa.s respectively. The black oil parameters used in ECLIPSE100 were calculated using CO_2 densities from the Span and Wagner (1996) equation-of-state (see Table 1) using the scheme described by Hassanzadeh et al. (2008).

Table 1
Representative CO_2 fluid properties used in the code comparison. The values were calculated using the Span and Wagner (1996) equation-of-state. Note that TOUGH2 uses correlations published by Altunin (1975) to obtain CO_2 fluid properties, however the two formulations show excellent agreement within the PT range of the case-studies. These properties were converted into black oil tables for ECLIPSE using the scheme described by Hassanzadeh et al. (2008).

Depth	Temperature (C)	Pressure (MPa)	Density ($\mathrm{kg \, m^{-3}}$)	Viscosity (cP)
700	25.6	7.3	745.81	0.0620
750	27.2	7.8	740.85	0.0613
800	28.8	8.3	736.25	0.0607
850	30.3	8.8	733.39	0.0604
900	31.9	9.3	729.37	0.0599
950	33.5	9.8	725.62	0.0594
1000	35.1	10.4	725.41	0.0594
1050	36.7	10.9	722.04	0.0590
1100	38.3	11.4	718.89	0.0586

1.4. The case-study simulations

Four case-study simulations have been used for our code comparison, each of which was based around aspects of the Sleipner CO_2 injection operation described above. The first case-study aimed to approximate whole plume geometry in a vertically heterogeneous reservoir using a 2D radial axisymmetric model. The second case-study investigated the temporal evolution of the topmost CO_2 layer in three-dimensions (see Chadwick and Noy (2010) for more information). This model is similar to the 'Sleipner Benchmark' released by Statoil in 2011 and described by Singh et al. (2010) and Cavanagh (2013). In the third case-study the TOUGH2 simulator was compared with an analytical solution for a single CO_2 layer spreading beneath a flat caprock. The final case-study, a simple axisymmetric model of a warm buoyant CO_2 plume rising upward through a uniform sandstone reservoir, was used to test the thermal modelling capabilities of two of the codes (PFLOTRAN and TOUGH2).

2. Case-study 1: 2D axisymmetric model code comparison

2.1. Model setup

The axisymmetric model for the full Sleipner plume used here has previously been described by Chadwick et al. (2010) and Chadwick and Noy (2015). It was created for the TOUGH2 simulator and incorporates a 2D radial axisymmetric mesh, with 80 cells in the X (I) grid direction increasing in width logarithmically with distance from the injection well. The mesh is only one cell thick in the Y (J) direction, but the cell volume increases with X so that it represents the full circumference at the radial distance X from the injection well.

The simulation grid is divided vertically into 170 cells with variable dimensions, chosen to give detailed resolution in the vicinity of the injection point and to include the thin mudstone layers known to trap CO_2 in the reservoir. The top of the reservoir is positioned at a depth of 797 m below sea level, with the base of the reservoir at 1083 m. No-flow boundary conditions were placed at the top, base and perimeter of the model, although the grid extends to a radial distance of 2.5×10^5 m, effectively behaving as an "open aquifer" over the injection timescale.

The geological model comprises 16 stratigraphical layers: four 'lower' sands and five 'upper' sands, with intervening thin mudstones and the topmost sand unit capped by 50 m of very low permeability caprock (Table 2). Sand permeabilities are consistent with measurements of 1.6–3.3 Darcy from a single core (Zweigel et al., 2004) but

Table 2
Rock units and physical properties used in the code comparison.

Property	Caprock	Upper Sand	Lower Sand	Intra-Reservoir Mudstone
Porosity ($-$)	0.17	0.37	0.37	0.17
Permeability (Darcy)	1.01325×10^{-7}	3.03975	1.01325	1.31722×10^{-1}
Van Genuchten λ ($-$)	0.4	0.75	0.75	0.7
Slr ($-$)	0.2	0.05	0.05	0.05
Sgr ($-$)	0.05	0.05	0.05	0.05
Capillary entry pressure (Pa)	2×10^6	1.5×10^3	1.5×10^3	1.65×10^4

modified following Chadwick and Noy (2015). The permeability of the intra-reservoir mudstones was adjusted to allow CO_2 to reach the top of the reservoir by 1999, matching time-lapse seismic observations which showed that CO_2 had reached the caprock just prior to the (October) 1999 repeat survey. This constraint has resulted in a much higher effective permeability for the intra-reservoir mudstones than has been measured on intact core samples of Sleipner caprock (around 4.0×10^{-7} Darcy, Harrington et al., 2010; Chadwick and Noy, 2015). This 'semi-permeable' behaviour might reflect preferential flow through pervasive small-scale fractures resulting in very low effective threshold pressures (Cavanagh and Haszeldine, 2014) or higher permeability feeder chimneys in the mudstones (Hermanrud et al., 2009).

Relative permeability and capillary pressure curves for CO_2 and brine in the Utsira Sand were computed by fitting a Van-Genuchten model to measurements from core samples measured in the laboratory (Eric Lindeberg personal communication). A similar function was used for the mudstones, but with an order-of-magnitude increase in capillary entry pressure (see Table 2 and Fig. 3).

A variable injection rate with a mean value of 27 kg s^{-1} was used, based on the actual values measured at the wellhead (Ola Eiken, Statoil, personal communication, see Fig. 3d).

2.2. Results

Sample results from the axisymmetric model comparison are presented as CO_2 saturation profiles extracted at simulation time-steps corresponding to the 1999, 2001 and 2006 seismic monitor surveys (Fig. 4). For comparison with the observed data, markers show the equivalent radial extent of each seismically mapped CO_2 layer, calculated by fitting a circle with the same area as the observed layer area. It is clear that the different codes produce remarkably consistent CO_2 distributions in the plume, with individual layer spreading very consistent between the models. The models also provide a reasonable match to the layer extents mapped on seismic data but it is noticeable that with time the modelled radii tend to progressively outstrip the observed equivalent radii. This is to be expected, given that layer spreading in the axisymmetric model is beneath perfectly flat mudstone seals, whereas the real seals have a degree of undulation, with buoyant ponding tending to retard spatial spread.

The relative consistency of each simulator in terms of advective fluid mass transfer through the plume can be tested using the volumetric growth of the topmost CO_2 layer and it is clear that the codes all show excellent agreement in predicting this (Fig. 5). CO_2 volume in the topmost layer can also be derived from time-lapse seismic analysis (see Chadwick and Noy, 2015 for methodology) and it is clear that the model results are consistent with seismic observations, with the proviso that very thin CO_2 accumulations at low saturation (< 0.2) cannot be reliably mapped on the time-lapse seismics (to account for this, only CO_2 saturations > 0.2 have been included in the simulated layer

volume curves).

3. Case study 2: 3D model code comparison

3.1. Model setup

Recent quantitative seismic analysis of CO_2 plume migration at Sleipner has focused on the topmost spreading layer in the plume (e.g. Chadwick and Noy, 2015; Williams and Chadwick, 2012; Furre et al., 2015). This layer lies directly beneath the reservoir caprock and is clearly and stably imaged on time-lapse 3D seismic data, which provides reliable constraints for flow simulation.

The monitoring data show that growth of the topmost layer between 1999 and 2006 was accomplished by rapid lateral spreading of CO_2 to infill a topography of domes and ridges beneath the reservoir topseal (Fig. 6).

The geological model for the code comparison is based on that developed by Chadwick and Noy (2015) and comprises a single uniform sand unit, 16 m thick, with a porosity of 0.37 and a permeability of 8 Darcy. Relative permeability and capillary pressure curves for CO_2 and brine in the Utsira Sand were computed by fitting a Van-Genuchten model to measurements from core samples measured in the laboratory (Table 2 and Fig. 3a). The assigned permeability is substantially higher than core-plug measurements (~ 3 Darcy), but recent re-assessment of regional permeability and wireline log data suggest that the permeability of the topmost sand body might be significantly higher than previously supposed (Williams and Chadwick, 2017). This is examined further in the Discussion.

The top reservoir surface was mapped from the baseline (1994) seismic dataset and depth-converted using a layer-cake velocity model derived from available well data. The model was discretised using 60 50×50 m cells along the X axis and 111 50×50 m cells along the Y axis. The 16 m thick reservoir was divided vertically into 8 $\times$ 2 m cells. No-flow boundary conditions were placed at the top and base of this layer (simulating an impermeable caprock and underlying mudstone layer), while the lateral model domains were maintained at near hydrostatic pressure conditions. This was achieved by using large boundary cells (TOUGH2 and PFLOTRAN) or a pore-volume multiplier (ECLIPSE).

The flow model assumed a single feeder to the top layer of CO_2 positioned at the prominent gas chimney observed on seismic data (Fig. 2), with CO_2 flux matched to volumes derived from the seismic data (Fig. 5). Temperature in the sand unit was set to 29C in the simulators and fluid properties were again calculated using the Span and Wagner (1996) equation-of-state in ECLIPSE and PFLOTRAN and Altunin's (1975) correlations in TOUGH2 (Table 1).

3.2. Results

Results from the three models show the extent of the top spreading layer at the time of the 2006 time-lapse seismic survey (Fig. 7). All models show the dual effects of radial spreading from the CO_2 source/feeder with evidence of buoyancy-driven migration in the north-east where the CO_2 is starting to migrate northwards beneath the linear ridge (Fig. 6).

As before, all three codes show good agreement in CO_2 distributions but with some variation in local migration patterns at the layer edges. In the Eclipse 100 simulation more CO_2 has spilled beyond the CO_2-water contact at the eastern margin of the grid compared to the TOUGH2 or PFLOTRAN models. This reflects the fact that Eclipse 100 is a black oil simulator that assumes a constant reservoir temperature. This was set to the average temperature in the layer (~ 30C), whereas a temperature gradient was used in the TOUGH2 and PFLOTRAN model runs. All of the simulation models are consistent with each other, but in absolute terms they fail to match the observed extents of layer spreading; this aspect is examined further in the Discussion.
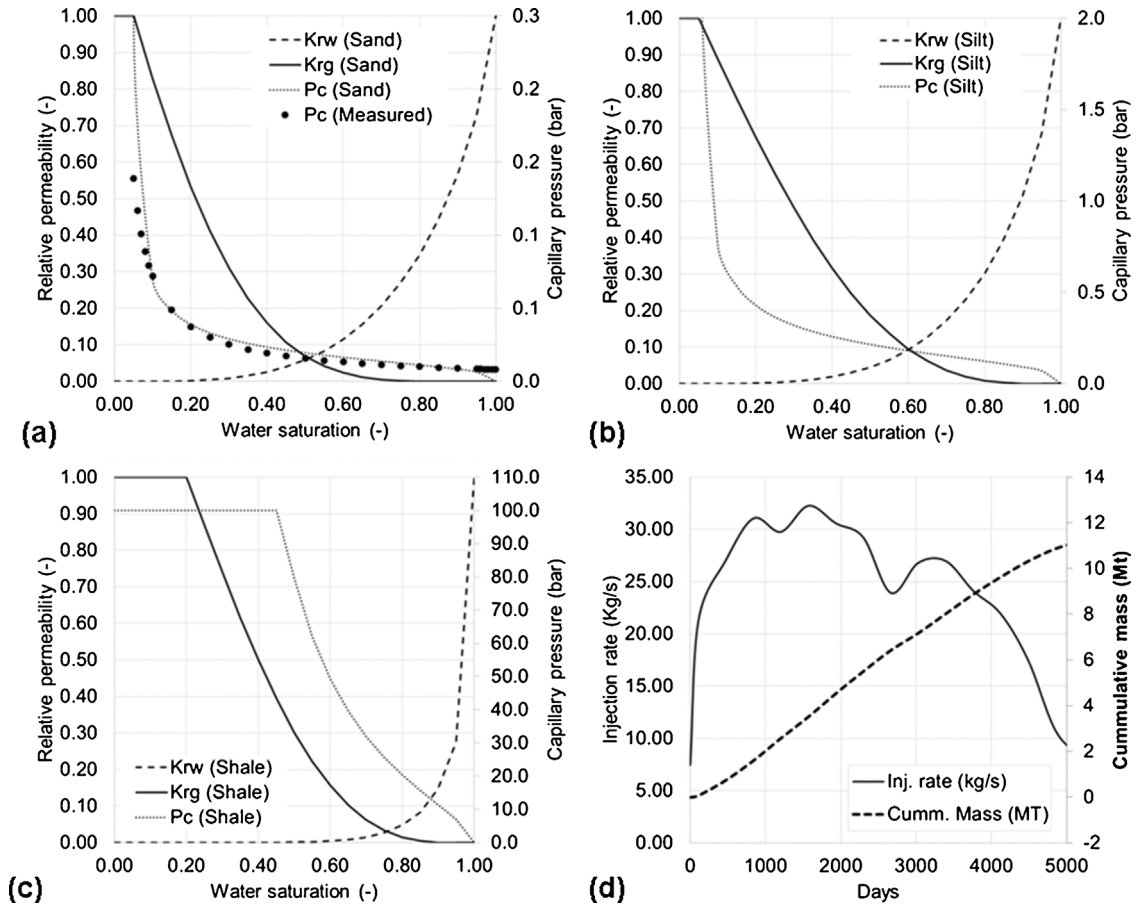
Fig. 3. (a) Relative permeability and capillary pressure curves for the Utsira sandstone. (b) Relative permeability and capillary pressure curves used for the silt/shale layers separating the individual sandstone bodies. (c) Relative permeability and capillary pressure curves for the caprock. (d) The injection rate as a function of time used in the 2D axisymmetric model.

4. Case-study 3: comparison of numerical codes with an analytical solution

The third case-study compares the numerical simulations with an analytical solution employing similar but simplified physics for the spreading of a single CO_2 layer beneath a flat caprock.

4.1. Analytical solution

Lyle et al. (2005) and Bickle et al. (2007) presented analytical solutions for gravity flows in a permeable medium with axisymmetric symmetry. Their model (Fig. 8) comprises a porous permeable medium filled with a fluid into which a less dense fluid is introduced along a line source under an impermeable caprock. The fluid ponds under the caprock and spreads radially. To obtain the solution several simplifying assumptions were made, including no capillary pressure, no viscosity difference, no relative permeability effects and constant fluid densities.

Darcy's Law and the continuity (conservation of mass) equation give key relationships between the rate of fluid input ($\alpha Q t^{(\alpha-1)}$, where a value $\alpha = 1$ corresponds to release at constant flux Q (m³/s)), the radius of the spreading layer, $rN(t)$ (m), as a function of time t (s), and the thickness of the layer h (m) as a function of radial distance r (m), and time (s).

The radius of the layer is given by:

$$r_{N(t)} = \eta_N(\alpha)(\gamma Q/\phi)^{\frac{1}{4}} t^{(\alpha+1)/4} \tag{1}$$

And the thickness is given by:

$$h(r, t) = \eta_N^2 \left(\frac{Q}{(\phi\gamma)}\right)^{\frac{1}{2}} t^{(\alpha-1)/2} f(y) \tag{2}$$

Where:

$$\gamma = \frac{\rho k g'}{(\phi\mu)}$$

$\emptyset$ is the porosity, k is permeability (m²), ρ is the density of the introduced fluid (kg/m³), μ the viscosity of the introduced fluid (Pa s) and $g' = g\Delta\rho/\rho$, the reduced gravity with $\Delta\rho$ the difference in density between the introduced fluid and the initial fluid filling the medium (kg/m³). The similarity variable η is given by:

$$\eta = \left(\frac{\gamma Q}{\phi}\right)^{-\frac{1}{4}} r t^{-(\alpha+1)/4}$$

$\eta_N (\alpha)$ (i.e. η at $r = r_N$) is a function of α only and is given by:

$$\eta_N = \left[2\pi \int_0^1 y f(y) dy\right]^{-\frac{1}{4}}$$

Where the scaled similarity variable $y = \eta/\eta_N$ ranges from 0 at the source to 1 at the outer edge of the CO_2 layer and $f(y)$ is given by numerical solution of the differential equation:

$$\frac{d}{dy}\left(y f \frac{\delta f}{\delta y}\right) + \frac{1}{4}(1+\alpha)y^2\frac{\delta f}{\delta y} + \frac{1}{2}(1-\alpha)y f = 0$$

Given:

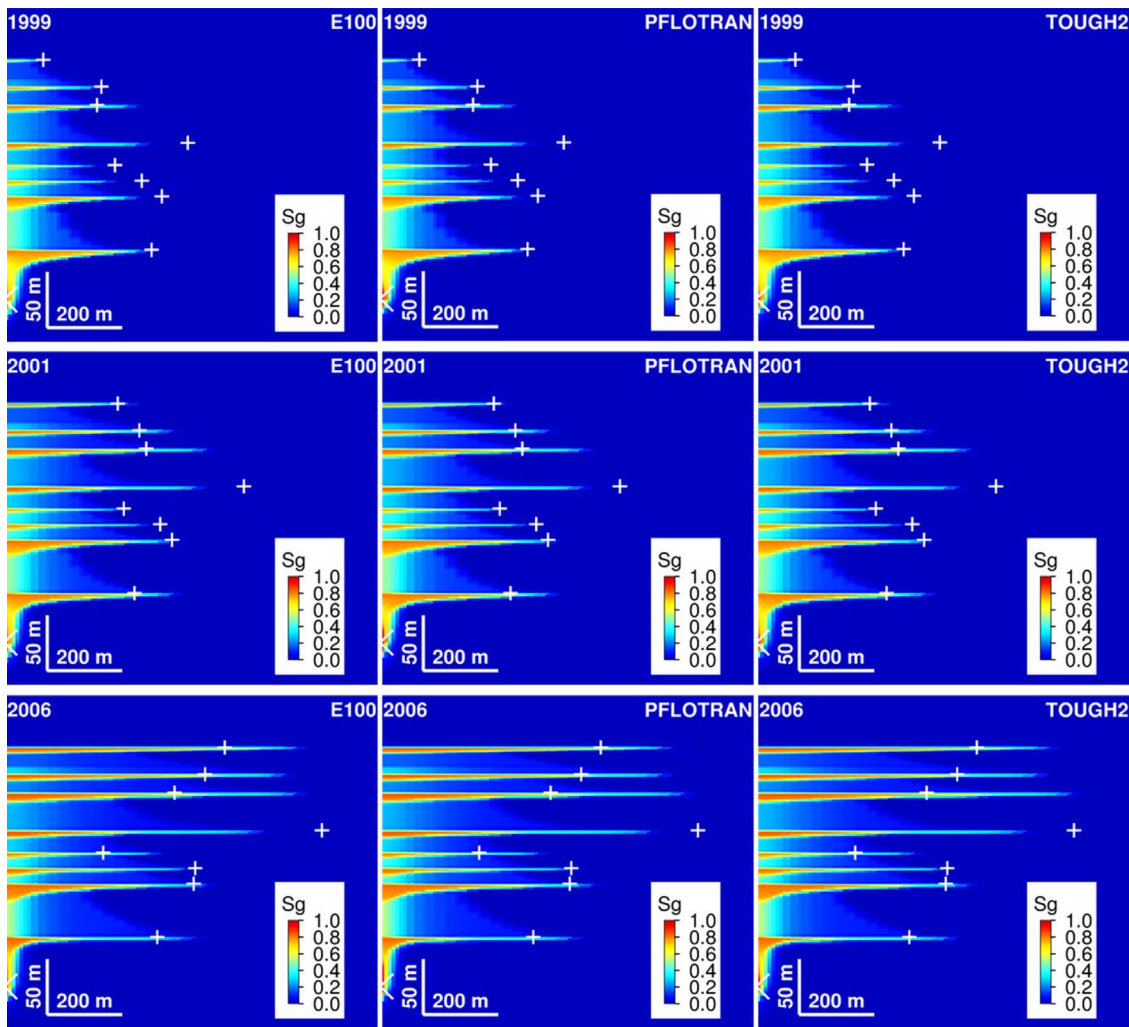$$f = \frac{1}{4}(1+\alpha)(1-y)(y \to 1)$$

Fig. 4. CO_2 saturation profiles for the 2D axi-symmetric code comparison. Simulation time-steps corresponding to the 1999, 2001 and 2006 seismic surveys are shown for each code used in the comparison. The grid cell containing the injection point is marked with an arrow in the lower left corner of each plot. White markers show the equivalent radial extent of each seismically mapped layer.
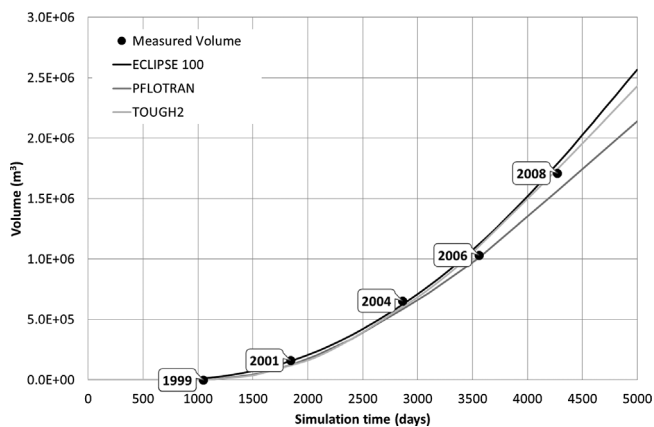

Fig. 5. Volumetric growth of the topmost CO_2 layer. Solid lines show volumes calculated from the axisymmetric plume models with a CO_2 saturation cut-off of 0.2. Black circles show CO_2 layer volume estimated from time-lapse seismic measurements.

Fig. 6. Perspective view of the top reservoir (base topseal) surface, looking north. Coloured polygons show the mapped extents of the topmost CO_2 layer in 1999 (solid white line), 2001 (black line) and 2006 (broken white line). Note the prominent north-trending linear ridge demarcated by the layer extents in 2006. Distance from the southern tip of the 2006 polygon to the northern tip is about 3000 m.
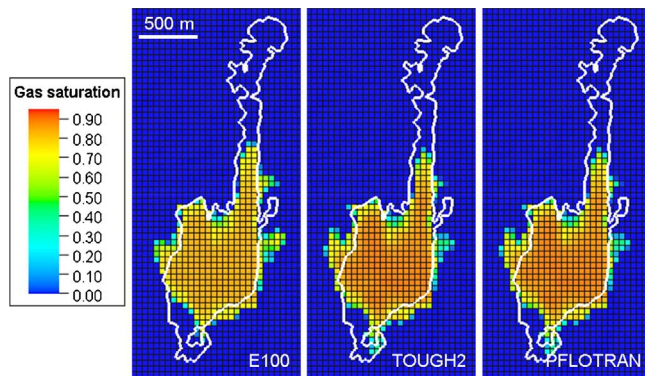
This is a good approximation for f except when y is small, and η_N is well approximated by:

$$\eta_N = \left[\frac{12}{\pi(1+\alpha)} \right]^{\frac{1}{4}}$$

Fig. 7. Extents of the topmost CO_2 layer in 2006, some 2500 days after the start of layer initiation in 1999. The bold white polygon delimits the lateral extent of the CO_2 layer mapped on 3D seismic data.
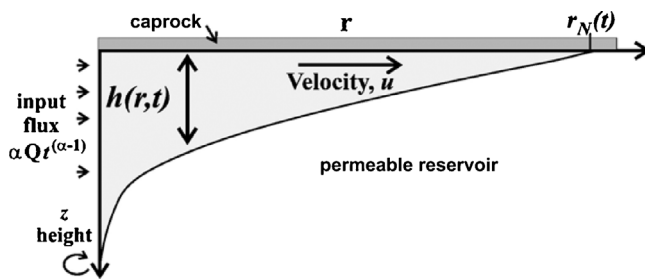

Fig. 8. Geometry and parameters of the layer spreading model (modified from Bickle et al., 2007).

The equations predict, that 1) for constant input flux ($\alpha = 1$) the radius of the CO_2 layer will be proportional to the square root of time; 2) for constant flux the axial thickness of the layer $h(0,t)$ is nearly invariant; 3) there are simple relationships between both the radius and thickness of the layer and the input flux and physical parameters porosity, viscosity and permeability.

4.2. Numerical model setup

The numerical simulation of a single CO_2 layer was carried out in TOUGH2. An axisymmetric model was setup injecting dense-phase CO_2 into the base of an aquifer 112 m thick with an impermeable caprock. The mesh is highly refined, with elements 5 cm thick at the top of the aquifer and 1 m wide out to a radius of 250 m, then gradually expanding to the outer boundary at 20 km.

Key properties of the model are based broadly on Sleipner (Table 3), with fluid properties as follows: brine salt mass fraction 0.032; brine density 1020 kg m^{-3}; brine viscosity 8.60×10^{-4} Pa s; CO_2 density 720 kg m^3; CO_2 viscosity 5.93×10^{-5} Pa s. The injection point was placed 102 m below the reservoir top with an injection rate of 10 kt per year, the latter being of the same order as the CO_2 supply to the topmost layer at Sleipner.

The analytical model assumes identical reservoir and fluid properties and conditions as the numerical model, with a constant flux of 10 kt per year of CO_2 along an axial line source (Fig. 9).

Table 3
Physical properties used in the numerical – analytical comparison.

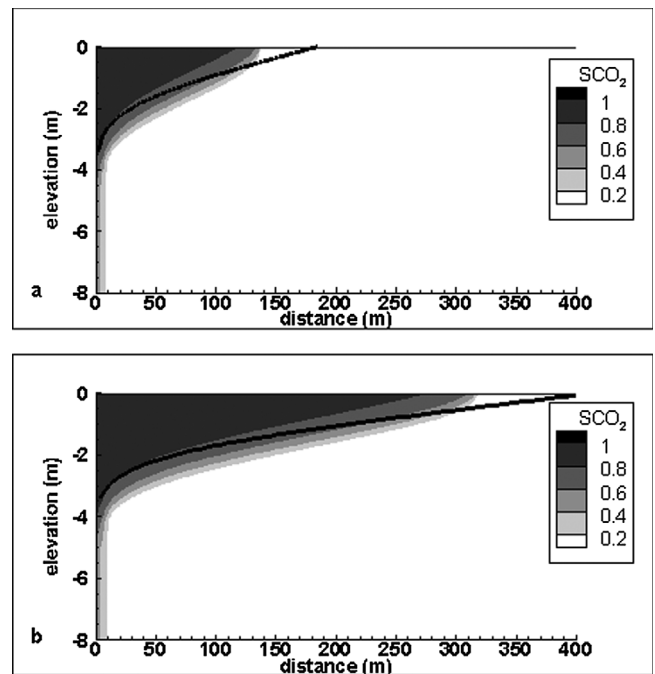| Physical Properties	Value
Caprock permeability (m^2)	0.0
Sand porosity ($-$)	0.37
Sand permeability (m^2)	1.00×10^{-12}
Hydrostatic pressure (MPa)	8.0
Reservoir temperature (°C)	29

Fig. 9. Growth of a single CO_2 layer with an injection rate of 10 kt y^{-1} Layer spread after 2 (a) and 10 (b) years from the numerical model with layer profiles from the analytical solution shown as black lines (Eq. (2)).

4.3. Results

In the TOUGH2 model the CO_2 rises in a thin buoyant column to the base of the caprock and then spreads radially beneath it (Fig. 9). The modelled layer is around 3–4 m thick in the axial part (above the feeder column) thinning gradually towards its leading-edge. A steepening of the CO_2–water contact (CWC) towards the perimeter is an effect of capillary resistance to flow of the CO_2, defined by the capillary pressure curve. CO_2 saturations in the layer, again defined by the capillary pressure curve, are generally high, but decrease towards the CWC across a zone termed the capillary fringe. The analytical model (shown as a black curve in Fig. 9) shows similar layer development and geometry to the numerical model but with significant differences. The CWC maintains a roughly uniform dip out to the layer edge and the layer spreads rather further than in the numerical model. Full CO_2 saturation throughout the layer is implicit in the analytical model, because it does not include capillary effects. Volumetrics require therefore that the layer in the analytical model be somewhat thinner than in the numerical model. The analytical solutions predict that for a constant injection rate the axial thickness of the layer is invariant (Eq. (2)). This behaviour is supported by the numerical model which maintains roughly constant axial layer thicknesses through time (Fig. 9).

To examine the effects of capillary forces on layer geometry and saturation a second scenario was developed, this time injecting 500 t of CO_2 per year (Fig. 10). A lower injection rate was selected because capillary effects are relatively more significant in thinner layers and the reduced injection rate provides this.

The first numerical model run included capillary pressure and shows a familiar geometry with the CWC steepening towards the layer edge with a saturation fringe (Fig. 10a). It is notable that the axial layer thickness is smaller than those above, reflecting the smaller input flux. The corresponding analytical model shows the familiar thinner layer with somewhat wider spread and uniform CWC dip (shown as a black line in Fig. 10a). The second numerical model run omitted capillary pressure effects from the computation (Fig. 10b). The resulting layer has full CO_2 saturation throughout and shows a much improved match to the analytical model in terms of both the layer spread and layer
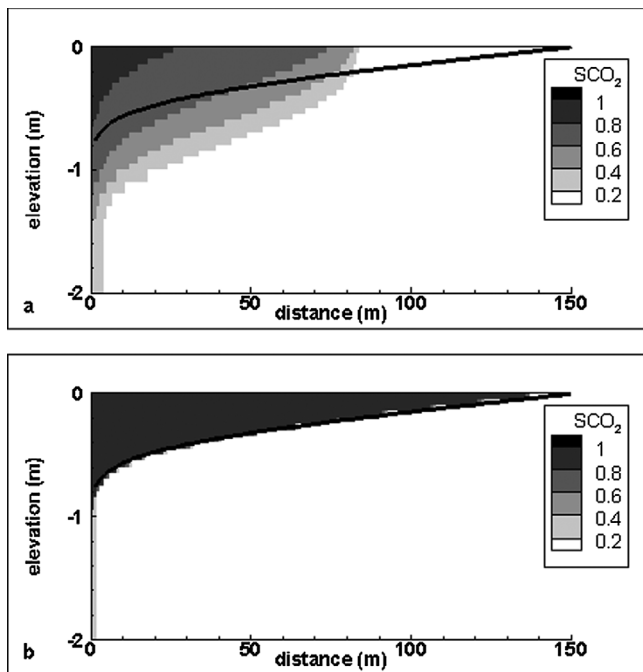
Fig. 10. Growth of a single CO_2 layer with an injection rate of 500 ty^{-1} a) Numerical model with capillary pressure b) Numerical model without capillary pressure. The black line in a, b shows the CO_2-water contact predicted by the analytical solution.

geometry.

In order to test for the effects of numerical dispersion, the model mesh was modified such that the cell heights at the top of the reservoir were increased from 5 cm to 25 cm (Fig. 11). Compared to the detailed numerical model this had the effect of increasing the volume of each modified grid cell and increasing the minimum layer thickness. One consequence is to reduce the free phase CO_2 saturation in the layer (Fig. 11b) because the same amount of CO_2 is distributed within a
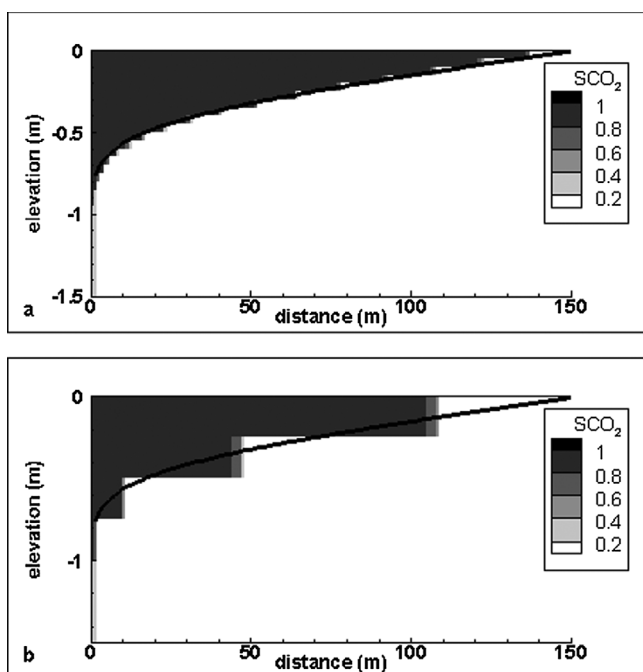

Fig. 11. The effects of numerical dispersion on growth of a single CO_2 layer with an injection rate of 500 ty^{-1} a) CO_2 saturation after 6 years for a model with a mesh spacing of 100 × 5 cm at the top of the reservoir b) CO_2 saturation after 6 years for a model in which the grid cell height has been increased from 5 to 25 cm.

greater volume in each cell. Another consequence is to reduce the layer lateral spread at the top of the plume. This is an important point because accurate modelling of lateral plume migration is a key requirement for robust long-term storage prediction. It is notable that even in the modified model (Fig. 11b) the layers are still very thin compared with cell dimensions typically adopted for generalised reservoir flow modelling, so this numerical dispersion effect is likely to be significant in many flow models.

To further the numerical/analytical comparison, repeat model runs were carried out in Eclipse 100 and PFLOTRAN with results that were, to all intents and purposes, identical to those from TOUGH2. It is evident therefore that, at least for the growth of a single layer, the numerical and analytical approaches give very comparable results. In the numerical models, capillary pressure effects clearly influenced layer geometries and saturations, especially for thinner layers, but when these were removed (to match the analytical model assumptions), results were almost identical.

5. Case-study 4: thermal effects

Much of the flow simulation work traditionally carried out for CCS assumes, for simplicity, that CO_2 is injected at ambient reservoir conditions. This is not usually the case. Depending on wellhead temperature and specific adiabatic conditions in the wellbore, CO_2 will generally not have the same temperature as the reservoir at the injection perforations. So, for example, when injecting into strongly depleted fields, adiabatic decompression in the wellbore will lead to injecting CO_2 significantly colder than the reservoir. In contrast, at Sleipner adiabatic compression in the wellbore leads to the injection of CO_2 warmer than the surrounding reservoir. The temperature of the CO_2 at the injection perforations is estimated at ~48C or slightly above (Alnes et al., 2011), around 13C warmer than ambient reservoir temperature at the injection point. Furthermore, interpretation of the time-lapse gravity data (Alnes et al., 2011) suggest that the average density of the CO_2 plume at Sleipner is compatible with its having a warm, less dense, axial core.

The effects of a plume of warm buoyant CO_2 rising to the top of the reservoir without cooling to ambient reservoir temperature are worthy of investigation. Two of the codes compared in this study (TOUGH2 and PFLOTRAN) solve for conservation of energy and are suitable for modelling heat propagation in a migrating CO_2 plume.

A new axisymmetric model was set up, injecting CO_2 at a rate of 27 kg s^{-1}, but at 49C, into the base of a homogeneous sandstone reservoir 275 m thick and overlain by 750 m of low permeability shale caprock (Table 4). This is simpler than the model shown in Fig. 4 in that there are no intra-reservoir mudstones to interrupt the plume ascent to the reservoir top.

The CO_2 saturation distributions produced by the two simulators in this simple reservoir model are to all intents and purposes identical (Fig. 12), a simple buoyant axial column of CO_2 rising above the injection point and feeding a single CO_2 layer spreading radially beneath the caprock.

Fluid temperature distributions from the two models are also very

Table 4
Rock units and physical properties used in the thermal code comparison.

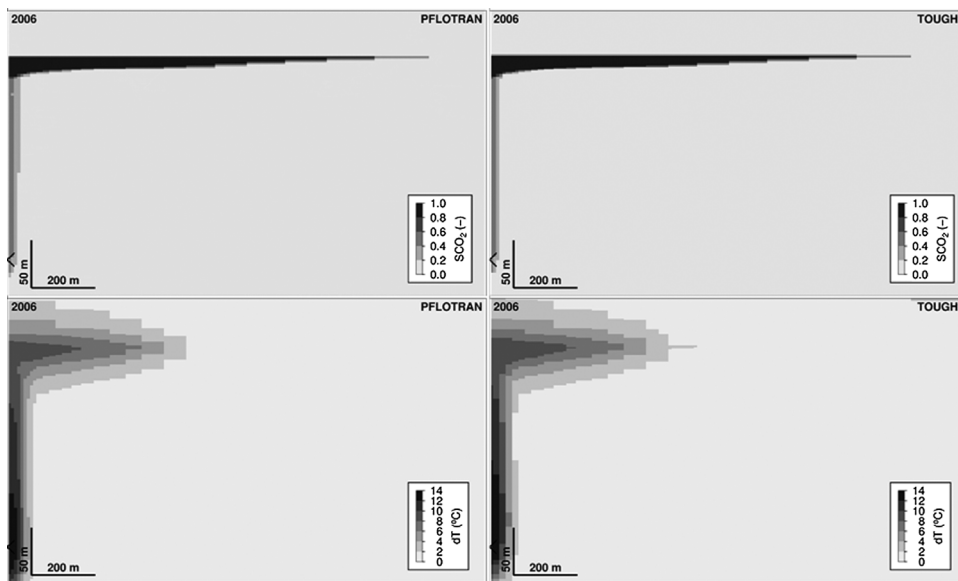| Physical Properties	Value
Caprock porosity (−)	0.17
Caprock permeability (Darcy)	1.01325×10^{-7}
Caprock thermal conductivity (W/m/K)	4.2
Caprock specific heat capacity (J/Kg/K)	1.0 + 03
Sand porosity (−)	0.37
Sand permeability (Darcy)	3.03975
Sand thermal conductivity (W/m/K)	4.2
Sand specific heat capacity (J/Kg/K)	1.0 + 03

Fig. 12. CO_2 saturation (PFLOTRAN top left, TOUGH2 top right) and thermal anomaly (PFLOTRAN bottom left, TOUGH2 bottom right) resulting from CO_2 injection into a homogeneous sandstone reservoir. The output time is equivalent to that of the 2006 seismic monitor survey. The grid cell containing the injection point is marked with an arrow in the lower left corner of each plot.

similar, comprising an axial column of elevated fluid temperatures above the injection point and a radially spreading thermal anomaly at the reservoir top. It is noticeable that the thermal imprints of the rising column and the spreading layer are of lesser spatial extent than the corresponding fluid saturation features. This is because of radial heat loss from the column into the surrounding reservoir and vertical heat loss from the spreading layer into the caprock and underlying reservoir. The thermal anomaly at the injection point is +14C, corresponding to the temperature difference between the injected CO_2 and the ambient reservoir. Above the injection point the temperature anomaly reduces to +8C at the reservoir top and reduces further radially, such that it becomes negligible at distances more than about one third of the full layer spread

More detail of the temperature evolution is revealed by a vertical temperature profile through the grid cells immediately above the injection point at a distance of 2.5 m from the model axis (Fig. 13a). Both codes show a consistent temporal and spatial evolution of the thermal anomaly. The dominant physical processes occurring in the model are rapid vertical advection of warm CO_2 combined with cooling due to expansion as the hydrostatic pressure drops with elevation above the injection point. Steady-state heat transfer occurs after ~365 days, and thereafter the vertical temperature profile closely approximates the Joule-Thomson (JT) cooling curve (Fig. 13a) with a coefficient of 5C/MPa for the warm buoyant CO_2 (Span and Wagner, 1996).

The models show that cooling due to expansion is significant and takes place a lot faster than conductive heat transfer to the surrounding reservoir. The CO_2 has cooled to a temperature of ~37C by the time it has reached the top of the reservoir (some 8C above the background reservoir temperature) and the thermal anomaly propagates laterally beneath the caprock for a distance of 700 m from the axis (Fig. 13b).

Because this particular model scenario is based on Sleipner which is a shallow reservoir with the injected CO_2 close to its Critical Point, the effect of the thermal anomaly on CO_2 properties (Fig. 14) is significant. A ~50% decrease in viscosity and density in the core of the plume both contribute to increased mobility of the CO_2 phase. The bulk modulus (Fig. 14d) is also markedly reduced which will modify the seismic properties of the CO_2. This will affect the rock physics of CO_2 saturated reservoir rock and should be taken into account for quantitative analysis of the seismic response such has been attempted a number of times at Sleipner (e.g. Chadwick and Arts, 2005; Furre et al., 2015).
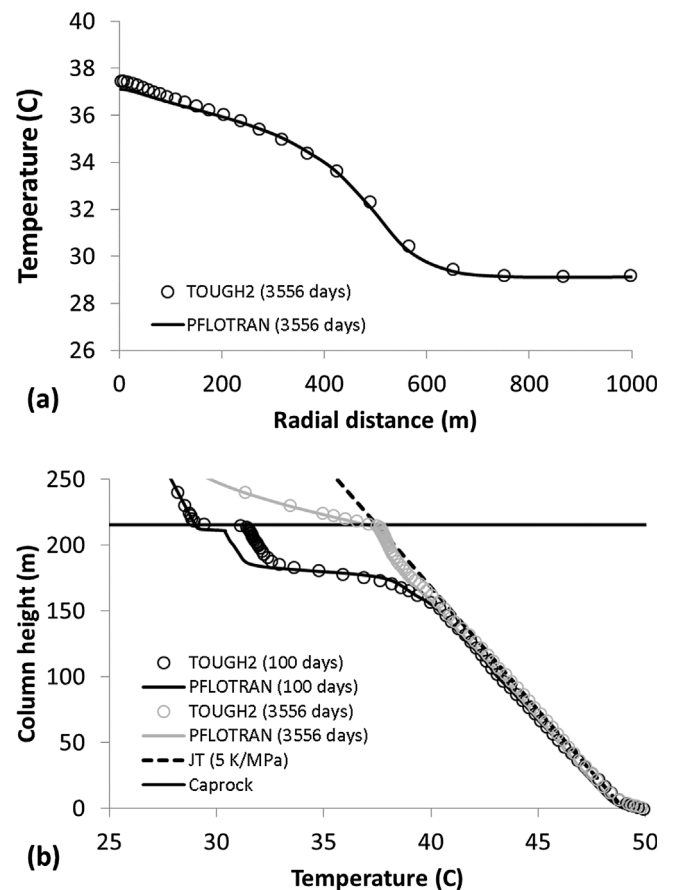

(a)

(b)

Fig. 13. (a) Vertical temperature profile at a distance of 2.5 m from the model axis, showing the temporal evolution of temperature with depth toward a steady-state solution, which was established by ~365 days following the onset of injection. (b) Comparison of the horizontal temperature distribution in the model cells immediately beneath the caprock 3556 days after the onset of injection (corresponding to the 2006 seismic monitor survey). JT = Joule-Thomson.

6. Discussion

6.1. Validity of Darcy-flow assumption

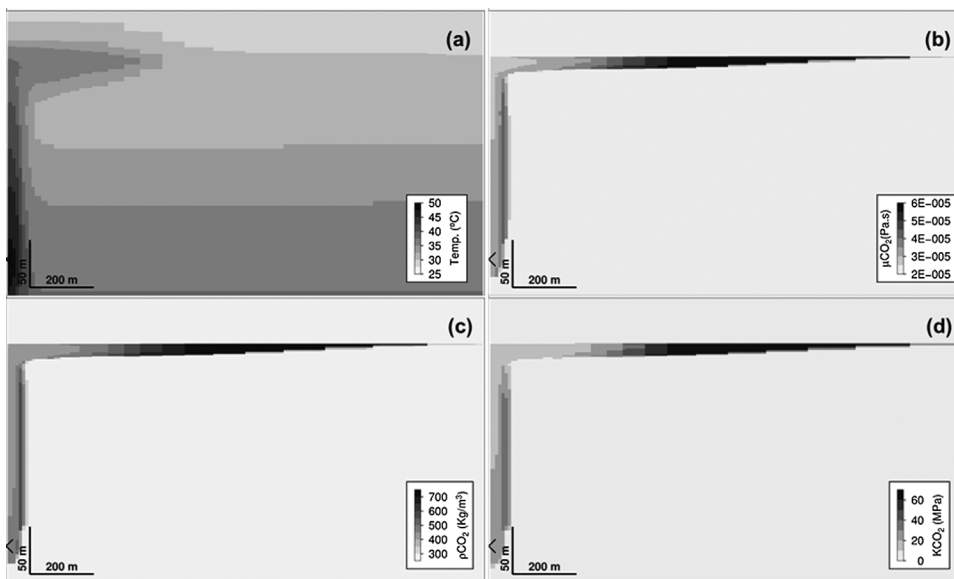The three simulators show results that are remarkably consistent

Fig. 14. (a) Thermal anomaly, (b) CO_2 viscosity, (c) CO_2 density and (d) CO_2 bulk modulus resulting from CO_2 injection into a homogeneous sandstone reservoir. The output time is equivalent to the 2006 seismic monitor survey. The grid cell containing the injection point is marked with an arrow in the lower left corner of each plot.

with each other. Differences in the modelled outer edges of the layer extents are generally around 50 m or less, though locally up to ~100 m. This is similar to or less than the uncertainty of layer edge detection on the seismic data itself, Bickle et al. (2007) noting that the outermost parts of the seismically-imaged layers would not be detectable due to their being too thin, with under-estimation of layer extents by up to 100 m. In absolute terms however none of the simulation case-studies match the observed monitoring data very well, notably in their failure to reproduce the rapid lateral spread of the layer observed by 2006. History-matching the observed growth of this layer has proved challenging generally, with most published simulations having difficulty with predicting the rapid northward migration of CO_2 along the prominent linear ridge in the base of the topseal (Figs. 6 and 7). Various authors have investigated the effects of small uncertainties in feeder geometry, topseal topography, permeability anisotropy and gas composition (e.g. Chadwick and Noy, 2015; Zhu et al., 2015) but the Darcy-based modelling approaches have had mixed results in replicating the observed layer growth rates.

Our numerical and analytical models are all based around a 'Darcy' type flow formulation. It has been proposed that because CO_2 migration in the topmost layer is dominated by buoyancy, rather than pressure-driven viscous forces, Darcy-type flow models, strictly valid only for slow viscous fluid flow, might not be wholly appropriate and modelling with alternative physics should be utilised (Cavanagh, 2013; Cavanagh and Haszeldine, 2014). In this context flow models with alternative physics have been proposed, notably the invasion-percolation (IP) scheme (Cavanagh, 2013). At Sleipner, IP modelling allows good spatial/geometric matching of the topmost layer spread, but it is a quasi-static technique that does not incorporate a temporal element (the fluid overcomes capillary resistance essentially instantaneously) and so is not well suited to the type of temporal history-matching that time-lapse monitoring requires (Oldenburg et al., 2015). Recent laboratory experiments (Krishnamurthy et al., 2017) comparing core-flood CO_2 saturation measurements against Darcy and IP simulations have found a tendency for IP to markedly underestimate CO_2 saturations, leading Krishnamurthy et al. (2017) to suggest hybrid modelling approaches, such as using multiple IP runs to pre-condition reservoir grid properties (e.g. capillary threshold pressure variation) prior to full Darcy simulation. More fundamental modelling approaches, reaching down into pore-scale processes, are also being developed, such as Lattice-Boltzmann modelling (e.g. Sukop and Thorne, 2007) but these are computationally very demanding and not currently suitable for simulating two-phase flows in reservoirs with complex geology and high resolution

geological characterisation datasets.

Recent support for the Darcy-based modelling approach is provided by detailed re-assessments of the reservoir properties at Sleipner (Williams and Chadwick, 2017, Cowton pers. comm.) which indicate significant depositional heterogeneity in the top reservoir sand, with wide permeability variation. When these more heterogeneous reservoir properties are incorporated into Darcy flow models a much closer history-match can be obtained (Williams and Chadwick, 2017).

It is clear that computing power is a primary limit on simulation accuracy, notable in limiting the resolution and geological detail that can be incorporated into the reservoir meshes. Our comparison shows marked differences in processor requirements between different Darcy simulators, but it is also clear that Darcy modelling is susceptible to useful simplifications and the vertical equilibrium approximation for numerical modelling has proved useful in simulating the Sleipner plume (e.g. Nilsen et al., 2011). More radical is the development of purely analytical solutions to model CO_2 flow (e.g. Nordbotten et al., 2005; Lyle et al., 2005; Bickle et al., 2007). These allow extremely rapid computation of layer flows, albeit in a simple reservoir, and our comparison shows that published analytical solutions are consistent with a full physics Darcy numerical model. More recently a hybrid approach has been developed, whereby analytical solutions for gravity flows beneath dipping seals have been discretised within a finite-difference numerical scheme to allow very short computational times even on a PC (Laurence Cowton pers. comm.). This level of computational efficiency allows the incorporation of complex geology at the small (metres) length scales that are really required for realistic modelling.

There is therefore a crucial trade-off between including full complex physics in flow models and the need to include complex and high resolution geological heterogeneity. It seems that Darcy modelling with suitable simplifications to allow radically reduced computation times is the best way to proceed at the present time, particularly where geological uncertainty is significant and where the spread of a migrating CO_2 layer is accurately tracked through time.

The inclusion of thermal effects is clearly important, and is rarely included in CO_2 plume simulation. For injection into depleted gas fields CO_2 entering the reservoir will generally be significantly cooler than the surroundings and accurate modelling of the evolving CO_2 front will be essential. Even in the normally-pressured aquifer of the Utsira Sand, temperature has an important effect on fluid mobility Williams and Chadwick (2017), and as we show here, potentially on the seismic response of the fluid-rock system.

6.2. Model runtimes

ECLIPSE 100 is at least 10 times faster than either PFLOTRAN or TOUGH2. This large difference in performance reflects the fact that both PFLOTRAN and TOUGH2 use numerical differentiation for the solution of the non-linear problem, while ECLIPSE uses analytical derivatives. This can bring significant computational saving. In addition TOUGH2 and PFOTRAN do not implement a linear solver optimised for the type of multi-phase problems encountered in reservoir simulations. ECLIPSE uses a nested factorisation that can offer significant speedup compared to standard linear solvers.

7. Conclusions

Three numerical multiphase flow simulators, one black-oil (ECLIPSE100) and two fully compositional (PFLOTRAN and TOUGH2), were tested on their ability to model CO_2 injection into a saline aquifer. Modelling case-studies were based on the Sleipner injection operation, which provided an appropriate context for large-scale storage, in terms of CO_2 layer dimensions, thickness profiles and spreading rates, plus excellent time-lapse monitoring data. All case-studies were set-up carefully on the three simulators to virtually eliminate 'operator effects'.

The simulators all showed excellent agreement in modelling the upward flux of CO_2 through an isothermal heterogeneous reservoir and in each case modelled saturation profiles showed good agreement with the distribution of CO_2 observed on time-lapse seismic surveys. 3D models of the topmost CO_2 layer, migrating beneath the caprock, and clearly imaged by seismic data, also showed excellent consistency between the three codes. Minor differences related to solver implementations, meshing, smoothing and small equation-of-state discrepancies. In all cases modelling differences were less than monitoring uncertainty. In absolute terms however none of the case-studies produced close matches of the layer's temporal evolution, notably its rapid lateral migration and very high mobility. One possibility is that the physics of fluid flow in this layer is different to the Darcy physics used by the simulators, but our favoured explanation is that imperfect reservoir characterisation is the root cause.

Numerical simulations of a simple, thin spreading layer with an analytical model also showed an excellent match and highlighted the effects of capillary forces in terms of layer fluid saturation and geometry. The importance of fine-scale modelling was also evident, as coarser numerical meshes resulted in strong numerical dispersion with impaired layer spreading accuracy.

Two of the codes (TOUGH2 and PFLOTRAN) were also run in non-isothermal mode to investigate the effects of injecting CO_2 significantly warmer than the ambient reservoir temperature. Again, the codes showed excellent agreement in predicting the distribution and magnitude of the resulting thermal anomaly and its temporal development. It is clear that, particularly in shallow reservoirs where stored CO_2 is close to its Critical Point, thermal effects are significant, because they affect CO_2 mobility and also its seismic properties, important for quantitative monitoring.

Acknowledgements

References

Alnes, H., Eiken, O., Nooner, S., Sasagawa, G., Stenvold, T., Zumberge, M., 2011. Results from Sleipner gravity monitoring: updated density and temperature distribution of the CO_2 plume. Energy Procedia 4, 5504–5511. http://dx.doi.org/10.1016/j.egypro.2011.02.536.

Altunin, V.V., 1975. Thermophysical Properties of Carbon Dioxide. Publishing House of Standards, Moscow.

Arts, R.J., Chadwick, R.A., Eiken, O., Thibeau, S., 2008. Ten years' experience of monitoring CO_2 injection in the Utsira Sand at Sleipner, offshore Norway. First Break 26, 65–72.

Baklid, A., Korbøl, R., Owren, G., 1996. Sleipner Vest CO2 disposal, CO2 injection into a shallow underground aquifer. In: SPE Paper 36600, Presented at 1996 SPE Annual Technical Conference and Exhibition. Denver Colorado, USA, 6–9 October 1996.

Bickle, M., Chadwick, A., Huppert, H.E., Hallworth, M., Lyle, S., 2007. Modelling carbon dioxide accumulation at Sleipner: implications for underground carbon storage. Earth Planet. Sci. Lett. 255, 164–176. http://dx.doi.org/10.1016/j.epsl.2006.12.013.

Cavanagh, A.J., Haszeldine, R.S., 2014. The Sleipner storage site: capillary flow modeling of a layered CO_2 plume requires fractured shale barriers within the Utsira Formation. Int. J. Greenh. Gas Control 21, 101–112. http://dx.doi.org/10.1016/j.ijggc.2013.11.017.

Cavanagh, A., 2013. Benchmark calibration and prediction of the Sleipner CO_2 plume from 2006 to 2012. Energy Procedia 37, 3529–3545. http://dx.doi.org/10.1016/j.egypro.2013.06.246.

Chadwick, R.A., Noy, D.J., 2015. Underground CO_2 storage: demonstrating regulatory conformance by convergence of history-matched modeled and observed CO_2 plume behavior using Sleipner time-lapse seismics. Greenh. Gas Sci. Technol. 5, 305–322. http://dx.doi.org/10.1002/ghg.1488.

Chadwick, R.A., Zweigel, P., Gregersen, U., Kirby, G.A., Johannessen, P.N., 2004. Characterisation of a CO_2 storage site: the Utsira sand, Sleipner, northern North sea. Energy 29, 1371–1381 (Elsevier Science Ltd, Oxford).

Chadwick, R.A., Arts, R., Eiken, O., 2005. 4D seismic quantification of a growing CO2 plume at Sleipner, North Sea. In: Dore, A.G., Vining, B. (Eds.), Petroleum Geology: North West Europe and Global Perspectives - Proceedings of the 6th Petroleum Geology Conference. Petroleum Geology Conferences Ltd. Published by the Geological Society, London. pp. 1385–1399.

Chadwick, R.A., Noy, D., Arts, R., Eiken, O., 2010. Latest time-lapse seismic data from Sleipner yield new insights into CO_2 plume development. Energy Procedia 1, 2103–2110. http://dx.doi.org/10.1016/j.egypro.2009.01.274.

Chadwick, R.A., Williams, G.A., White, J.C., 2016. High resolution imaging and characterisation of a CO_2 layer at the Sleipner CO_2 Storage operation using time-lapse seismics. First Break 34, 79–87.

Class, H., Ebigbo, A., Helmig, R., Dahle, H., Nordbotten, J., Celia, M., Audigane, P., Darcis, M., Ennis-King, J., Fan, Y., Flemisch, B., Gasda, S., Jin, M., Krug, S., Labregere, D., Beni, Naderi, Pawar, A., Sbai, R., Thomas, A., Trenty, S., Wei, L., 2009. A benchmark study on problems related to CO_2 storage in geologic formations. Comput. Geosci. 13, 409–434. http://dx.doi.org/10.1007/s10596-009-9146-x.

Directive 2009/31/EC of the European Parliament and of the Council of 23 April 2009 on the Geological Storage of Carbon Dioxide and Amending Council Directive 85/337/EEC, European Parliament and Council Directives 2000/60/EC, 2001/80/EC, 2004/35/EC, 2006/12/EC, 2008/1/EC and Regulation (EC) No 1013/2006 (Text with EEA relevance).

Duan, Z., Sun, R., Zhu, C., Chou, I.-M., 2006. An improved model for the calculation of CO_2 solubility in aqueous solutions containing Na +, K +, Ca2 +, Mg2 +, Cl-, and SO42-. Mar. Chem. 98, 131–139. http://dx.doi.org/10.1016/j.marchem.2005.09.001.

Fenghour, A., Wakeham, W.A., Vesovic, V., 1998. The viscosity of carbon dioxide. J. Phys. Chem. Ref. Data 27, 31–44. http://dx.doi.org/10.1063/1.556013.

Furre, A.K., Kiær, A., Eiken, O., 2015. CO_2-induced seismic time shifts at Sleipner. Interpretation 3 (3), 23–35.

Harrington, J.F., Noy, D.J., Horseman, S.T., Birchall, D.J., Chadwick, R.A., 2010. Laboratory study of gas and water flow in the Nordland Shale, Sleipner, North Sea. In: Grobe, M., Pashin, J.C., Dodge, R.L. (Eds.), Carbon Dioxide Sequestration in Geological Media − State of the Science, AAPG Studies in Geology. AAPG, pp. 521–543.

Hassanzadeh, H., Pooladi-Darvish, M., Elsharkawy, A.M., Keith, D.W., Leonenko, Y., 2008. Predicting PVT data for CO2-brine mixtures for black-oil simulation of CO_2 geological storage. Int. J. Greenh. Gas Control 2, 65–77. http://dx.doi.org/10.1016/S1750-5836(07)00010-2.

Haywood, R.W., 1965. Sixth international conference on the properties of steam – release. J. Eng. Power 87, 93–98. http://dx.doi.org/10.1115/1.3678147.

Hermanrud, C., Andresen, T., Eiken, O., Hansen, H., Janbu, A., Lippard, J., Bols, H.N., Simmenes, T.H., Teige, G.M.G., 2009. Storage of CO_2 in saline aquifers: lessons learned from 10 years of injection into the Utsira Formation in the Sleipner area. Energy Procedia 1, 1997–2004. http://dx.doi.org/10.1016/j.egypro.2009.01.260.

Krishnamurthy, P.G., Senthilnathan, S., Yoon, H., Thomassen, D., Meckel, T., DiCarlo, D., 2017. Comparison of Darcy's law and invasion percolation simulations with

buoyancy-driven CO_2-brine flow in heterogeneous sandstone core. J. Petrol. Sci. Eng. 155 (2017), 54–62.

Lichtner, P.C., Hammond, G.E., Lu, C., Karra, S., Bisht, G., Andre, B., Mills, R.T., Kumar, J., 2015. PFLOTRAN User Manual.

Lyle, S., Huppert, H.E., Hallworth, M., Bickle, M., Chadwick, A., 2005. Axisymmetric gravity currents in a porous medium. J. Fluid Mech. 543, 293–302.

Nilsen, Møll, Halvor, Paulo A., Meisam Ashraf, Herrera, Ligaarden, Ingeborg., Iding, Martin, Hermanrud, Christian, Lie, Knut-Andreas, Nordbotten, Jan M., Dahle, Helge K., Keilegavlen, Eirik, 2011. Field-Case simulation of CO2 -Plume migration using vertical-Equilibrium models. 10th International Conference on Greenhouse Gas Control Technologies 4, 3801–3808. http://dx.doi.org/10.1016/j.egypro.2011.02.315.

Nordbotten, J.M., Celia, M.A., Bachu, S., 2005. Injection and storage of CO_2 in deep saline aquifers: analytic solution for CO_2 plume evolution during injection. Transp. Porous Med. 58, 339–360.

Oldenburg, C.M., Mukhopadhyay, S., Cihan, A., 2015. On the use of Darcy's law and invasion-percolation approaches for modelling large-scale geologic carbon sequestration. Greenh. Gas Sci. Technol. 5, 19–33. http://dx.doi.org/10.1002/ghg.1564.

Pruess, K., Oldenburg, C.M., Moridis, G.J., 1999. TOUGH2 User's Guide Version 2.

Pruess, K., 2004. The TOUGH codes: a family of simulation tools for multiphase flow and transport processes in permeable media. Vadose Zone J. 3, 738–746.

Pruess, K., 2005. ECO2N: A TOUGH2 Fluid Property Module for Mixtures of Water, NaCl, and CO2. Lawrence Berkeley National Laboratory Berkeley.

Schlumberger, 2011. Eclipse Technical Description. pp. 1 (2011).

Singh, V.P., Cavanagh, A., Hansen, H., Nazarian, B., Iding, M., Ringrose, P.S., 2010. Reservoir modeling of CO_2 plume behavior calibrated against monitoring data from Sleipner, Norway, in: SPE-134891-MS. Soc. Petroleum Eng. http://dx.doi.org/10.2118/134891-MS.

Span, R., Wagner, W., 1996. A new equation of state for carbon dioxide covering the fluid region from the triple-point temperature to 1100 K at pressures up to 800 MPa. J. Phys. Chem. Ref. Data 25, 1509–1596. http://dx.doi.org/10.1063/1.555991.

Spycher, N., Pruess, K., 2005. CO_2-H_2O mixtures in the geological sequestration of CO2. II. Partitioning in chloride brines at 12–100C and up to 600 bar. Geochim. Cosmochim. Acta 69, 3309–3320. http://dx.doi.org/10.1016/j.gca.2005.01.015.

Sukop, M.C., Thorne, D.T., 2007. Lattice Boltzmann Modeling: An Introduction for Geoscientists and Engineers, 2nd edition. Springer Berlin Heidelberg, New York.

Vesovic, V., Wakeham, W., Olchowy, A., Sengers, A., Watson, V., Millat, R., 1990. The transport properties of carbon dioxide. J. Phys. Chem. Ref. Data 19, 763–808. http://dx.doi.org/10.1063/1.555875.

Williams, G., Chadwick, A., 2012. Quantitative seismic analysis of a thin layer of CO_2 in the Sleipner injection plume. Geophysics 77, R245–R256.

Williams, G.A., Chadwick, R.A., 2017. An improved history-Match for layer spreading within the Sleipner plume including thermal propagation effects. In: 13th International Conference on Greenhouse Gas Control Technologies, GHGT-13. 14–18 November 2016, Lausanne, Switzerland. pp. 2856–2870. http://dx.doi.org/10.1016/j.egypro.2017.03.1406. 114 (Supplement C).

Zaytsev, I., Aseyev, G., 1992. Properties of Aqueous Solutions of Electrolytes. CRC Press.

Zhu, C., Zhang, G., Lu, P., Meng, L., Ji, X., 2015. Benchmark modelling of the Sleipner CO_2 plume: calibration to seismic data for the uppermost layer and model sensitivity analysis. Int. J. Greenh. Gas Control 43, 233–246. http://dx.doi.org/10.1016/j.ijggc.2014.12.016.

Zweigel, P., Arts, P., Lothe, A.E., Lindeberg, E.B.G., 2004. Reservoir geology of the Utsira Formation at the first industrial-scale underground CO2 storage site (Sleipner area, North Sea). In: In: Baines, S., Worden, R.H. (Eds.), Geological Storage for CO2 Emissions Reduction 233. Special Publications, Geological Society London, pp. 165–180.